



Research article

## Strategies for granule formation of mixed purple phototrophic bacteria culture in a photo-sequencing batch reactor



Siwei Yu<sup>a,b</sup>, Tianqi Hao<sup>a,b</sup>, Xiaoshuai Peng<sup>a,b</sup>, Yifeng Xu<sup>a,c</sup>, Linchuan Fang<sup>a,c</sup>, Lai Peng<sup>a,b,c,\*</sup>

<sup>a</sup> Key Laboratory of Green Utilization of Critical Non-metallic Mineral Resources, Ministry of Education, Wuhan University of Technology, Wuhan, 430070, China

<sup>b</sup> Shenzhen Research Institute of Wuhan University of Technology, Shenzhen, 518000, Guangdong, China

<sup>c</sup> Hubei Key Laboratory of Mineral Resources Processing and Environment, Wuhan University of Technology, Luoshi Road 122, Wuhan, 430070, China

ARTICLE INFO

Handling editor: Raf Dewil

Keywords:

Purple phototrophic bacteria (PPB) granules  
Photo-sequencing batch reactor (PSBR)  
Granulation  
Extracellular polymeric substances (EPS)  
Resource recovery

ABSTRACT

Purple phototrophic bacteria (PPB) are promising candidates for sustainable wastewater treatment and resource recovery due to their versatile metabolism and valuable biomass. However, their suspended growth and poor settleability hinder effective biomass retention and recovery. In this study, a photo-sequencing batch reactor (PSBR) was operated long-term to cultivate PPB granules through multiple strategies, including upflow velocity regulation and sodium, calcium, and magnesium ion addition. Under optimized conditions, PPB granules with excellent settling performance (77.98 m/h) and a median particle size of 255.48  $\mu\text{m}$  were successfully formed, while flocculent sludge was nearly eliminated. Increasing upflow velocity from 3.15 to 4.5 m/h improved particle size distribution (D90 increased from 533.19 to 896.88  $\mu\text{m}$ ). Sodium addition (5 g/L) enhanced granule adhesion by increasing extracellular polysaccharides (PS) content by 71.95 %, while calcium and magnesium (100 mg/L each) improved structural integrity by increasing extracellular protein (PN) content by 38.80 % and promoting uniformity. Microbial analysis revealed dynamic community succession, with *Rhodobacter* and *Psychrobacter* dominating in the later stage, and extracellular polymeric substances (EPS)-associated genera such as *Brevundimonas* and *Flavobacterium* contributing to granule stability. The system achieved a COD removal efficiency of 84.41 %, with a removal rate of 0.75 kg COD/m<sup>3</sup>/d under 2 d hydraulic retention time (HRT) and 0.9 kg COD/m<sup>3</sup>/d organic loading rate (OLR), showing comparable performance to previously reported PPB-based systems. In addition, PPB granules accumulated high-value products including proteins (39.91 %) and pigments (5.34 %), supporting their potential for wastewater resource recovery. This study provides insights into optimizing PPB granule formation and highlights the feasibility of PPB-based granular systems for practical applications.

### 1. Introduction

Purple phototrophic bacteria (PPB) are widely recognized for their potential in wastewater treatment and resource recovery due to their high biomass yields ( $\sim 1 \text{ g COD}_{\text{biomass}}/\text{g COD}_{\text{removed}}$ ) and relatively fast growth rates under anaerobic phototrophic conditions (Alloul et al., 2019; Hülsén et al., 2014). PPB utilize light energy to convert carbon, nitrogen, and phosphorus from wastewater into biomass rich in high-value substances such as proteins and pigments. However, the suspended growth characteristic of PPB presents significant challenges for downstream product recovery, which typically requires high-cost

separation processes such as sedimentation, membrane filtration, and centrifugation (Chen et al., 2020). These operations may account for 20–30 % of the total cost of wastewater treatment (Alloul et al., 2018). Although membrane technology has been applied to address solid-liquid separation challenges, additional biomass concentration steps remain necessary, limiting the overall economic feasibility of PPB-based processes (Cerruti et al., 2020).

Granular biomass, a specialized form of biofilm formed through microbial self-aggregation, offers superior settling ability and structural stability, providing a more cost-effective and easily recoverable alternative for PPB-based systems. Nevertheless, granule formation may also

\* Corresponding author. Key Laboratory of Green Utilization of Critical Non-metallic Mineral Resources, Ministry of Education, Wuhan University of Technology, Wuhan, 430070, China.

E-mail address: [lai.peng@whut.edu.cn](mailto:lai.peng@whut.edu.cn) (L. Peng).

introduce new challenges. It has been noted that the dense structure of granules may reduce light availability within the biomass, which is already a limiting factor in high-density suspended PPB cultures (Capson-Tojo et al., 2022). In addition, intrinsic physiological properties of PPB, such as their small size (0.4–2  $\mu\text{m}$ ) and limited extracellular polymeric substances (EPS) secretion, remain major obstacles to granule formation (Alloul et al., 2018; Capson-Tojo et al., 2020). Previous studies on PPB granulation are limited, recent findings on PPB biofilm growth suggest that PPB possess aggregation and attachment capabilities, raising the possibility of granule formation (Capson-Tojo et al., 2023; Shaikh et al., 2023). Stegman et al. (2021) further demonstrated the feasibility of PPB granule formation under appropriate upflow velocities. The average settling velocity of PPB granule exceeded 30 m/h, comparable to that of existing granular technologies. Upflow velocity plays a key role in granule formation by enhancing cell-to-cell interactions. However, the influence of other environmental factors, such as substrate concentration and inorganic ion supplementation, have not yet been explored.

Several hypotheses have been proposed to explain microbial granulation, including the inert nuclei hypothesis, the selection pressure hypothesis, and the extracellular polymer bonding hypothesis (Liu et al., 2003). These theories suggest that granulation is a multifactorial process involving complex physicochemical and biological interactions (Gagliano et al., 2017). Among these, EPS secretion plays an important role, as bacteria become entangled and cross-linked by EPS to form stable aggregates. Divalent metal ions such as calcium and magnesium have been reported to enhance the coagulation capacity of EPS by neutralizing negative charges, thereby accelerating the granulation process (Liu et al., 2010; Ren et al., 2008). Their strong affinity for EPS further supports the structural integrity of granules. Sodium ions have been shown to promote the flocculation of *Rhodobacter sphaeroides*, yet the role in the granulation process of mixed PPB cultures remains unclear (Lu et al., 2019a). Moreover, granule formation is commonly accompanied by changes in the microbial community structure. It remains unknown whether microbial changes would affect recovery quality of PPB-derived resource products.

Therefore, this study focused on the formation of PPB granules and their resource recovery performance in a photo-sequencing batch reactor (PSBR). Various control strategies, including adjustments to chemical oxygen demand (COD) concentration, upflow velocity, and the addition of sodium, calcium, and magnesium, were employed during long-term cultivation. Granule characteristics such as particle size distribution, settling velocity, and EPS content were analyzed to evaluate granulation. COD removal and the accumulation of high-value biomass products (proteins and pigments) were quantified to assess the system's pollutant removal performance and resource recovery potential. In addition, microbial community composition and diversity were examined to elucidate microbial community dynamics. This work provides strategies for regulating PPB granule formation, offering novel insights for the application of PPB granule technology in wastewater treatment and resource recovery.

## 2. Materials and methods

### 2.1. Granule inoculum

In this study, biomass cultivation was conducted in a 2.0 L cylindrical plexiglass PSBR (diameter x height: 70 × 520 mm). The reactor was inoculated with a mixed PPB culture from a laboratory-scale reactor, which was dominated by *Rhodobacter sphaeroides* (~60%). The initial concentration of mixed liquor suspended solids (MLSS) was around 3 g/L. The reactor was fed with synthetic wastewater containing 1.92 g/L of sodium acetate (equivalent to a COD of 1500 mg/L), 0.3 g/L of  $\text{NH}_4\text{Cl}$ , 0.6 g/L of  $\text{KH}_2\text{PO}_4$ , 0.8 g/L of  $\text{K}_2\text{HPO}_4$ , 0.5 g/L of  $\text{MgCl}_2 \cdot 6\text{H}_2\text{O}$ , 0.1 g/L of  $\text{CaCl}_2 \cdot 2\text{H}_2\text{O}$ , 0.7 g/L of  $\text{Na}_2\text{SO}_4$ , 1.0 g/L of  $\text{NaCl}$  and 0.3 g/L of  $\text{NaHCO}_3$ . The COD:N ratio (~100:5) and  $\text{NH}_4\text{Cl}$  concentration were based on

values commonly used in PPB systems and previous studies (Hulsen et al., 2016; Meng et al., 2017). Additionally, 1 mL/L of trace elements solution and 1 mL/L of vitamins solution were added as described by Imhoff et al. (2006). The pH of influent wastewater was adjusted to approximately 7.0 using NaOH. After inoculation, the reactor was flushed with nitrogen gas for 10 min.

### 2.2. Reactor set-up and operation

To investigate the granulation process of PPB under defined conditions, the reactor was operated in sequencing batch mode. SBR systems provide periodic control over feeding, reaction, and settling, introducing hydraulic and settling selection pressures that facilitate the retention of fast-settling biomass. These features are particularly beneficial for PPB, which typically exhibit poor settling behavior in continuous systems. In addition, feast-famine cycles and short settling times are recognized as drivers of EPS production and microbial aggregation in granular systems (Salimi et al., 2015; Wilén et al., 2018), and have proven effective in PPB granulation (Stegman et al., 2021). To further support biomass suspension and enhance granulation, the system employed an upflow influent configuration.

The system was operated for ~300 days and divided into 6 operational stages (Table 1), with a schematic diagram provided in Fig. S1. Prior to stages V and VI, samples were collected from the reactor for preliminary experiments to evaluate the effects of sodium and divalent metal ions on biomass growth and EPS production. The results showed that supplementing the original medium with 5 g/L NaCl was suitable for both biomass accumulation and EPS synthesis, and this concentration was subsequently adopted for stage V. Similarly, the separate addition of 100 mg/L  $\text{CaCl}_2$  and  $\text{MgCl}_2$  was implemented as the metal ion addition strategy in stage VI (Fig. S2). In stage I, the reactor was operated at an upflow velocity of 2 m/h to support PPB adaptation. The hydraulic retention time (HRT) was 2 days, while the organic loading rate (OLR) and COD concentration were maintained at 0.75 kg COD/m<sup>3</sup>/d and 1500 mg/L, respectively. After the initial start-up, the upflow velocity was increased to 3.15 m/h (stage II). In stage III, the influent COD concentration was elevated, raising the OLR to 0.9 kg COD/m<sup>3</sup>/d. In stage IV, the upflow velocity was further increased to 4.5 m/h, followed by sodium and metal ion addition in stages V and VI, respectively.

The reactor was maintained at  $32 \pm 2^\circ\text{C}$  under room temperature conditions. Illumination was provided by three 40 W incandescent bulbs positioned approximately 20 cm from the side of the reactor, with irradiance of ~29 W/m<sup>2</sup> (details refer to Text S1). No optical filters were applied, and the lamp emission spectrum covered both visible and near-infrared regions relevant for phototrophic activity (Fig. S3). Notably, despite the presence of visible light, no green microalgae were observed throughout the experimental period, likely due to the anaerobic and organics-rich conditions maintained within the system, which are unfavorable for the proliferation of oxygenic phototrophs (Capson-Tojo et al., 2021; Lu et al., 2019b). To ensure an anaerobic environment, the reactor headspace was routinely flushed with nitrogen throughout the operation. Each cycle lasted 3 h, consisting of 2 min of feeding, 166 min of reaction, 10 min of settling, and 2 min of decanting. The reactor wall was scrubbed with a magnet every 2 days to resuspend any attached

**Table 1**  
The operations and settings at different stages.

Stage	Time (d)	Upflow velocity (m/h)	OLR (kg COD/m <sup>3</sup> /d)	Influent COD (mg COD/L)	HRT (d)	SRT (d)
I	0–23	2	0.75	1500	2	5.02
II	23–57	3.15	0.75	1500	2	4.91
III	57–98	3.15	0.9	1800	2	5.09
IV	98–162	4.5	0.9	1800	2	4.70
V	162–243	4.5	0.9	1800	2	8.96
VI	243–298	4.5	0.9	1800	2	7.95

biofilm. Influent was pumped from a refrigerated tank maintained at 4 °C to preserve its physicochemical properties. Samples were collected twice a week to measure VSS, SS, COD, crude protein, EPS, and pigments. The sludge retention time (SRT) was calculated based on the ratio of biomass loss (due to sampling and washing) to the biomass inventory (Table 1).

### 2.3. Analytic methods

The measurement of MLSS and mixed liquor volatile suspended solids (MLVSS) were conducted using standard methods (American Public Health Association, 2017). The polysaccharide and protein content in EPS were quantified using the anthrone-sulfuric acid method and the modified Lowry method (Kurzyna-Szklarek et al., 2022; Lowry et al., 1951). Pigments, including carotenoids and bacteriochlorophylls, were extracted using a mixture of acetone and methanol (7:2, v/v), following the method described by Yu et al. (2021). The absorbance of the extracts was measured using a spectrophotometer at 473 nm and 771 nm, respectively. Pigment concentrations were calculated using the following equations (Zhou et al., 2014):

$$\text{Carotenoids content} = A_{473} \times 10000 / (250 \times L \times W) \quad (1)$$

$$\text{Bacteriochlorophylls content} = A_{771} \times 10000 / (76 \times L \times W) \quad (2)$$

where  $A_{473}$  and  $A_{771}$  represent the absorbance at 473 nm and 771 nm, respectively; L is the cuvette pathlength (cm); and W is the sample's initial mass (g) divided by the volume (mL) of the extraction solvent.

Liquid samples were centrifuged at 10,000 rpm for 15 min using a benchtop centrifuge (Eppendorf 5430, Germany) to obtain the supernatant for COD, total nitrogen (TN) and total phosphorus (TP) analysis. The supernatant was then filtered through 0.45 μm membrane filters prior to measurement. COD was determined by the colorimetric method using potassium dichromate in sulfuric acid with a commercial test kit (LH-YDE-100, China). TN and TP were measured in accordance with the standard methods (American Public Health Association, 2017). The settling velocity of granules was assessed by recording the time required for granules to settle from a defined height in a measuring cylinder (Batstone and Keller, 2001). The biomass size distribution was analyzed using a particle size analyzer (Mastersizer, 2000; Malvern, UK). The morphology and surface structure of granule was observed using scanning electron microscope (SEM, JSM-7500F, Japan).

### 2.4. Microbial community analysis

Granule samples from photoreactor were collected at the end of each stage and genomic DNA was extracted from the biomass with a DNA extraction kit (DL2000, Magigene Biotechnology, China). The purity and concentration of the extracted DNA samples were assessed using NanoDrop One (Thermo Fisher Scientific, MA, USA). Microbial communities within the granules were analyzed based on 16S rRNA gene sequencing. The V4 hypervariable region was amplified by the polymerase chain reaction (PCR) using primer pair of 338F (5'-ACTCC-TACGGGAGGCAGCAG-3') and 806R (5'-GGACTACHVG GGTWTCTAAT-3') (Zhang et al., 2022a). DNA samples were stored at -20 °C before sequencing on the Illumina Miseq PE250 platform. The Illumina Miseq sequencing service and data analysis were provided by Magigene Biotechnology Co., Ltd. (Guangzhou, China). The beta diversity was assessed through principal coordinates analysis (PCoA) using a Bray-Curtis dissimilarity matrix.

### 2.5. Statistical analysis

Statistical analysis was conducted with SPSS 26.0. Significant differences were evaluated through one-way analysis of variance (ANOVA), with  $p < 0.05$  indicating statistical significance. PCoA was

carried out using the R package ropl (version 1.6.2).

## 3. Results and discussion

### 3.1. Granule formation process

To assess the granule formation process throughout the operational period, changes in biomass concentration, particle size and settling velocity are shown in Fig. 1. During stages I and II (days 0–57), the biomass concentration increased significantly following the reactor startup and increase in upflow velocity, reaching 3.15 g/L MLSS by day 57 (Fig. 1a). The VSS/SS ratio gradually decreased, indicating an increase in the proportion of inorganic ash in the biomass. It is probably due to the accumulation of phosphate and divalent cations (e.g.,  $\text{Ca}^{2+}$ ,  $\text{Mg}^{2+}$ ) from the synthetic influent and their interaction with EPS during granulation. The addition of excess phosphate to the influent in our study for pH buffering may have further promoted inorganic precipitation. Similar observations were also reported in the literature (Jiang et al., 2025; Li et al., 2019). Fig. S4 shows that the initial culture exhibited a bimodal size distribution, with approximately 37 % of the particles in the 0.2–2 μm range and 63 % in the 5–300 μm range. Additionally, the D90 value (the particle size below which 90 % of the particles fall) of the initial culture was 48.48 μm. Granule formation was first observed at the end of stage II. At this point, the proportion of biomass with particle sizes greater than 200 μm (defined as granules) reached 17.44 %, and D90 value significantly increased to 374.83 μm ( $p < 0.05$ ) compared to the initial stage (Fig. 1b and c). These findings indicate that the increase in upflow velocity facilitated the initial formation of PPB granules.

In stage III (days 57–98), a large accumulation of loosely flocculated sludge was observed as the OLR increased to 0.9 kg COD/m<sup>3</sup>/d, with biomass particles smaller than 10 μm accounting for 75 % of the total (Fig. 1c). This suggests that the upflow velocity was insufficient to sustain the granulation process, resulting in the accumulation of flocculated biomass and hindering granule formation. The D90 exhibited an initial increase followed by a decrease, which was consistent with the trend observed in the settling velocity. Therefore, in stage IV (days 98–162), the upflow velocity was increased to 4.5 m/h to facilitate the discharge of flocculated biomass from the system. Consequently, the MLSS concentration decreased to 2.40 g/L on day 162, while the D90 increased to 896.88 μm, with the proportion of particles larger than 200 μm rising to 39.70 %. The results indicate that the granulation process was recovered under the pressure of the elevated upflow velocity.

At the end of stage V (days 162–243), the median particle size (D50) was observed to reach 151.06 μm (Fig. 1b), comparable to PPB aggregate sizes reported in the literature (Cerruti et al., 2020). Meanwhile, the proportion of granules and settling velocity increased to 58.20 % and 61.56 m/h, respectively, indicating the regulatory effect of sodium addition on granule formation. Notably, fluctuations in particle size data at the end of this stage were caused by the faulty pump affecting sampling. In stage VI (days 243–298), an evident increasing trend in the MLVSS concentration was observed as shown in Fig. 1a. Calcium and magnesium have been reported to enhance microbial growth and proliferation as cofactors for key enzymes (Liu et al., 2010). During this stage, the D10 and D50 values of the particles increased steadily. In particular, the D50 value (average 203.99 μm, n = 6) was significantly higher than that of stage V (average 94.09 μm, n = 6,  $p < 0.05$ ), while the D90 value slightly decreased. The size distribution of the particles (Figs. S4 and 1b) further showed the proportion of particles smaller than 10 μm almost disappeared on day 298, with ~55 % of the particles lying in the 200–2000 μm size range and a median particle size of 255.48 μm. The effect of metal ions on the particle size may be associated with changes in the distribution of inorganic precipitates, which has been reported in related studies (Li et al., 2009). This inference was further supported by the decreased VSS/SS ratio observed in stage VI (Fig. 1a), which indicated an increased inorganic content within the granules. The elevated inorganic fraction might have contributed to the formation of

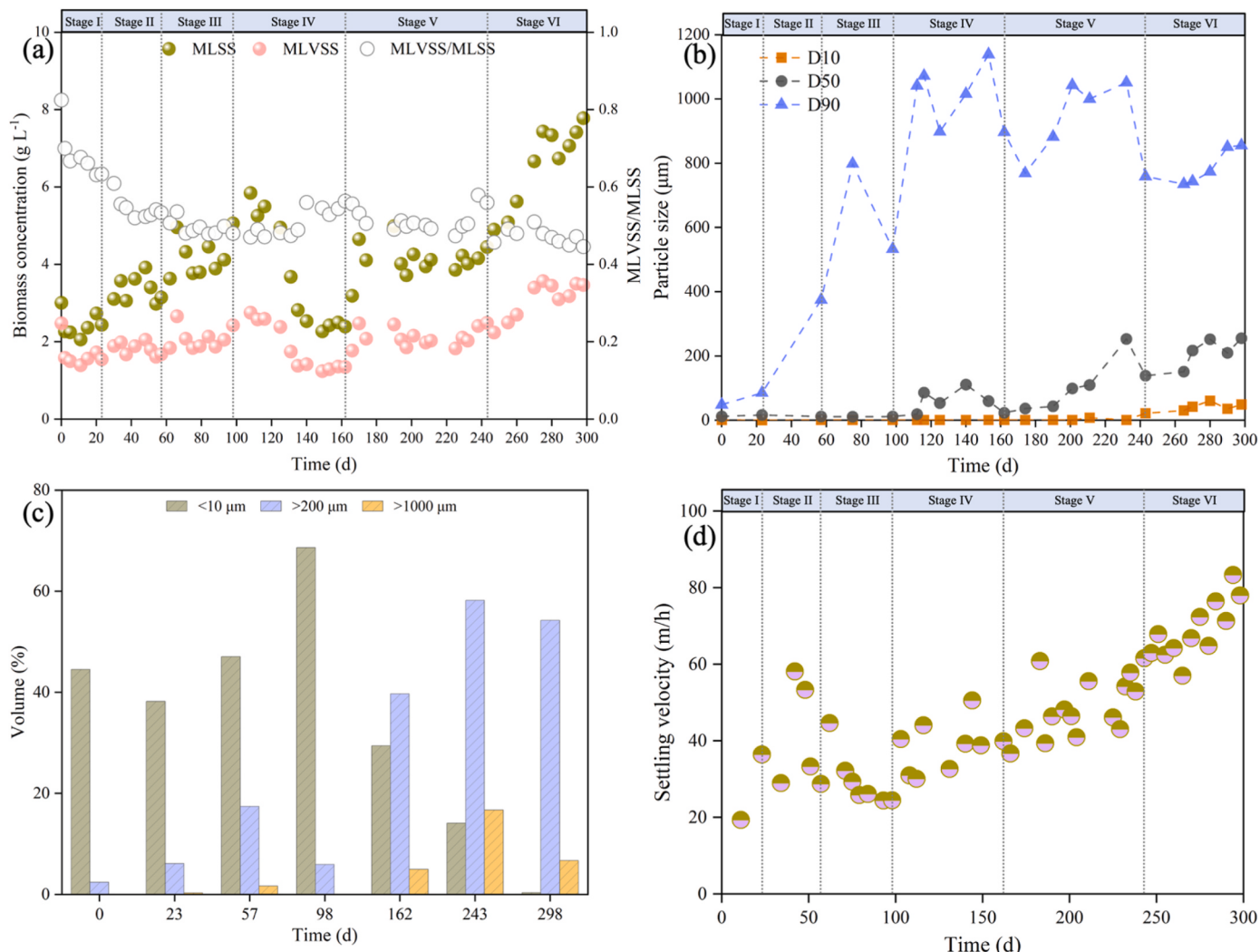


**Fig. 1.** Changes in (a) biomass concentration, (b) particle size, (c) size distribution, and (d) settling velocity during reactor operation. The six operational stages involved: acclimation (I), upflow velocity increase to 3.15 m/h (II), COD elevation (III), further upflow increase to 4.5 m/h (IV), sodium addition (V), and divalent metal ion addition (VI).

denser and more compact granule structures. Moreover, the settling velocity on day 298 reached 77.98 m/h, which exceeded the reported range for aerobic granular sludge (10–40 m/h) (Abouhend et al., 2018), indicating that the granulation process had stabilized. It suggests that calcium and magnesium additions regulated the particle size distribution, mainly promoting the aggregation of smaller bacteria and significantly improving the settling performance of the granules.

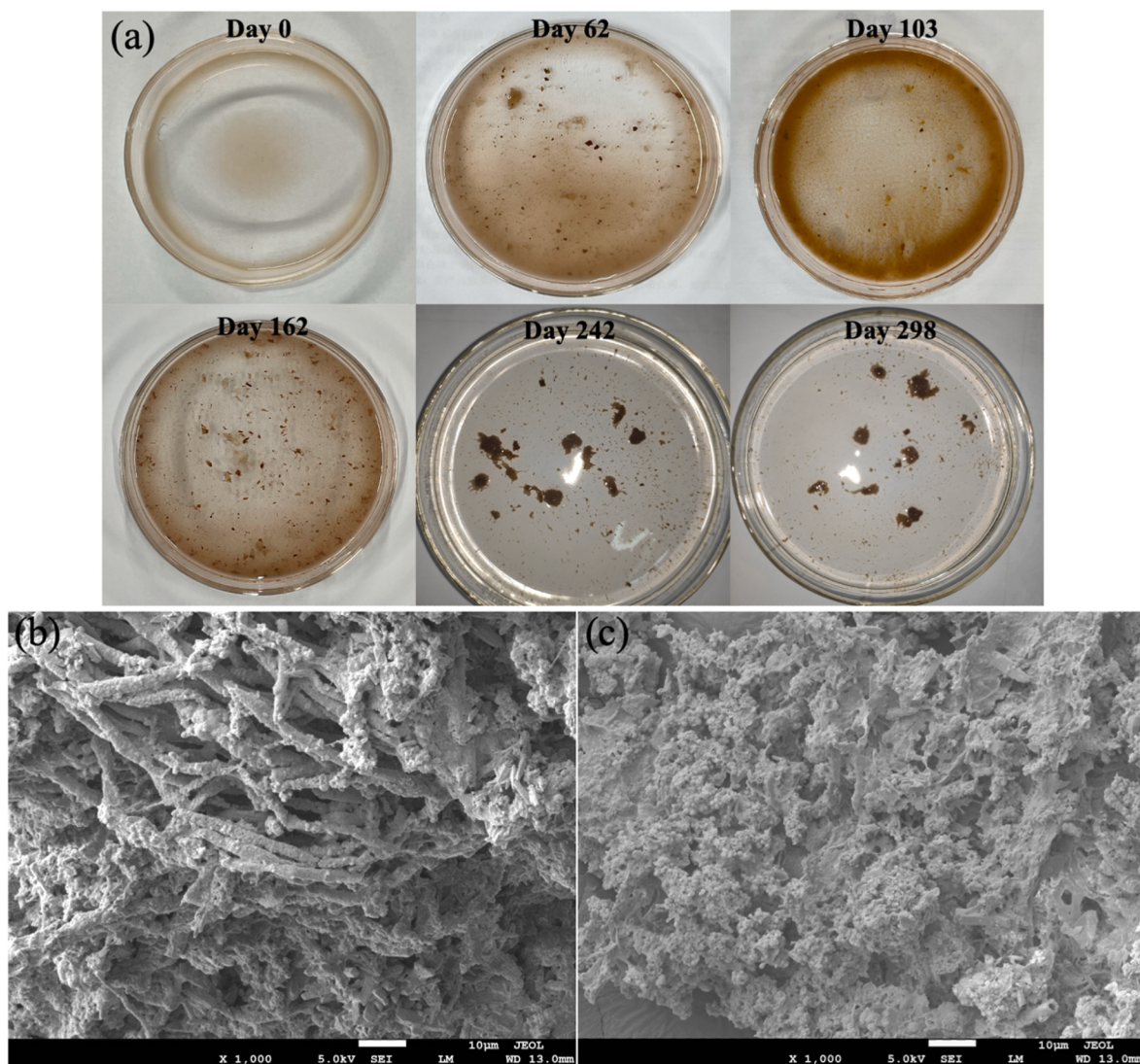
### 3.2. Granule morphology and EPS content

Fig. 2a shows the changes in bacterial morphology at each stage of reactor operation. Initially, the culture consisted of uniformly dispersed, fine bacteria. At the end of stage II (day 57), the formation of fine granules was observed, with loosely adhered flocculent sludge on the surface. As OLR increased (day 103), the proportion of loosely adhered flocculent sludge also increased. The increase in upflow velocity reduced the amount of flocculated sludge through scouring and decomposition, while fine granules were restored (day 162). With the addition of NaCl, flocculated sludge further decreased, and a distinct morphological transition of granules was observed in stage V (day 242). By day 298, the well-defined and morphologically stable granules had formed. However, the mature granules exhibited an irregular and loose structure, possibly influenced by the addition of sodium and metal ions. Meanwhile, the

culture color shifted from orange to yellow-brown, suggesting potential microbial community transitions during granulation, which will be further discussed in the following section.

The SEM images in Fig. 2b and c presents the surface morphology of granules during the stages of sodium ion addition (stage V) and divalent metal ion addition (stage VI), respectively. Granules in sodium addition stage exhibited a relatively smooth surface, with no obvious mesh or channel structures (Fig. 2b). This compact morphology may restrict substrate and nutrient diffusion and reduce light penetration into the granule interior, which is essential for sustaining phototrophic activity in PPB. In contrast, granules in divalent metal ions addition stage exhibited significant porosity and an intertwined mesh structure, with noticeable cracks and channels (Fig. 2c). Such porous structures are likely to enhance mass transfer and improve light availability within granules, potentially mitigating the adverse effects of light attenuation commonly observed in dense phototrophic systems. These microstructural differences aligned with the observed granule morphology in the reactor, indicating distinct effects of sodium and divalent metal ions. Sodium primarily influenced external granule characteristics, while divalent metal ions enhanced internal porosity and structural stability.

The viscous substance observed on granule surfaces in the SEM images is likely secreted EPS, which plays a crucial role in bacterial granulation. EPS is primarily composed of extracellular polysaccharides



**Fig. 2.** The bacterial morphology and structure. (a) Changes in bacterial morphology at different stages of reactor operation, (b, c) SEM images of granules at stages V (sodium addition) and VI (divalent metal ion addition), respectively.

(PS) and extracellular proteins (PN), which facilitate microbial aggregation and surface adhesion (Zhang et al., 2022b). Fig. 3 illustrates the changes in EPS content across different operational stages. During the initial two stages (days 0–57), EPS content increased from 93.74 mg/g VSS to 136.77 mg/g VSS, supporting the visual observation of granule formation at the end of stage II (Fig. 2a). Although an increase in OLR is generally expected to enhance EPS production (Torres et al., 2018), EPS levels stabilized during stage III. This may be related to the higher proportion of flocculated sludge at this stage, as granular biomass typically accumulates more EPS than flocculated sludge (Li et al., 2025). The EPS content gradually increased after increasing the upflow velocity in stage IV, while the PN/PS ratio decreased to an average of 1.46 ( $n = 9$ ), which corresponded to the recovery of the granulation process.

In stage V, sodium addition significantly enhanced EPS content, mainly by promoting PS synthesis. Compared to the previous stage, the average PS content increased by 71.95 % (from 55.03 to 94.62 mg/g VSS,  $p < 0.05$ ), which corresponded to the increase in median particle size and settling velocity (Fig. 1b and d). Under salt stress, microorganisms respond to elevated osmotic pressure by secreting additional EPS (Wan et al., 2014). The increased PS content not only enhanced microbial aggregation and adhesion but also improved granule stability by increasing surface hydrophilicity. A similar phenomenon has also

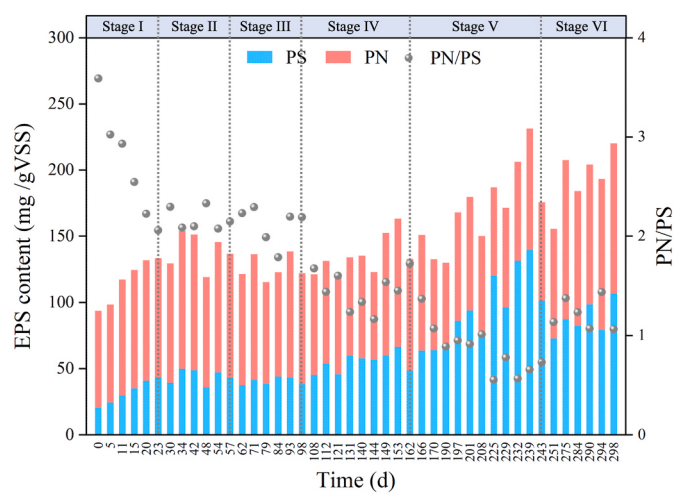


**Fig. 3.** Variations of EPS content in the reactor during the operation. The six stages represent: acclimation (I), upflow velocity increase to 3.15 m/h (II), COD elevation (III), further upflow increase to 4.5 m/h (IV), sodium addition (V), and divalent metal ion addition (VI).

been reported in anaerobic ammonia-oxidizing and algal-bacterial granules (Fang et al., 2018; Zhang et al., 2025). In stage VI, a distinct shift in EPS composition was observed. The average PN content increased by 38.80 % (from 76.60 to 106.31 mg/g VSS,  $p < 0.05$ ), while PS levels remained relatively stable. This was accompanied by a more uniform particle size distribution, with a reduction in large particles and the near disappearance of flocs (Fig. 1c). The PN/PS ratio rose to an average of 1.22 ( $n = 6$ ), comparable to values reported for mature microalgae-bacteria granules (Zhang et al., 2022b). The enrichment of PN likely contributed to enhanced granule compactness, as calcium and magnesium ions are known to cross-link EPS components and strengthen structural cohesion.

Overall, granule formation and structural modifications were closely linked to the regulation of EPS content and PN/PS ratio. The selection pressure exerted by the increasing upflow velocity promoted granulation, accompanied by a reduction in the PN/PS ratio and an increase in protein content. Sodium enhanced granule adhesion primarily by stimulating PS secretion, but this resulted in a more confined surface structure, which may have limited mass transfer efficiency. In contrast, calcium and magnesium facilitated the formation of a porous granule structure more conducive to mass transfer by interacting with EPS. These distinct mechanisms for granule optimization demonstrated synergistic effects in improving granule settling performance.

### 3.3. Microbial community structure

To explore variations in microbial diversity across different operational stages, alpha diversity indices (Simpson and Shannon for diversity, and Chao1 and ACE for richness) were analyzed based on high-throughput sequencing results (Table 2). The results revealed significant variations in microbial richness and diversity across different stages. The microbial richness and diversity increased in stages II and IV following adjustments to the upflow velocity. This may be attributed to moderate shear stress, which promoted the growth of specific microbial communities and enhanced biofilm formation through improved intercellular interactions and microbial selection. In contrast, an increase in OLR resulted in higher microbial diversity but lower richness, suggesting that the increased COD concentration supported microbial coexistence and improved community equilibrium. However, both microbial diversity and richness decreased in stages V and VI, indicating that the environmental stress induced by ion addition not only promoted the enrichment of functional microorganisms but also intensified competition among dominant populations.

PCoA analysis further confirmed significant shifts in microbial community structure throughout the operation (Fig. S5), with closer relationships between communities in stages II-IV and more distinct clustering in stages V and VI. As presented in Fig. 4, the reactor was initially dominated by *Rhodobacter* (60.4 %) and *Pseudomonas* (36.1 %) during the acclimatization period (stage I). Although *Pseudomonas* is generally classified as an obligate aerobe, previous studies have shown that certain strains can survive in anoxic environments by adopting alternative metabolic pathways, such as acetate fermentation via phosphotransacetylase and acetate kinase, as well as the glyoxylate shunt (Kolbeck et al., 2021; Trunk et al., 2010). Due to its metabolic

versatility and compatibility with reactor conditions, *Pseudomonas* was one of the dominant genera during the early operational stage. In stage II, the increased upflow velocity and limited light penetration led to substantial PPB washout, causing a rapid decline in PPB abundance to 20.5 %. In contrast, the EPS production and floc formation of *Pseudomonas* enabled it to better endure shear stress and be retained in the reactor (Ding et al., 2019). Some non-PPB genera, including *Brevundimonas* and *Flavobacterium*, gradually increased in abundance. These filamentous bacteria are commonly found in granular sludge and have been implicated in promoting structural stability during early granulation (Huang et al., 2024).

In stage III, although the increased OLR and appropriate carbon substrate supply facilitated the recovery of PPB abundance to 31.6 %, the proportion of flocculated sludge increased significantly. The 7.7 % increase in the abundance of unknown genera contributed to the rise in microbial diversity. As acetate-utilizing anaerobes became increasingly competitive, the abundance of other EPS-producing genera such as *Pseudomonas*, *Brevundimonas* and *Flavobacterium* declined. Additionally, rapid biomass growth exacerbated the issue of insufficient upflow driving force, further destabilizing the granular structure. After increasing the upflow velocity in stage IV, the intensified shear stress eliminated loosely bound flocs, leading to a 10 % decrease in unknown genera, a 5.3 % reduction in *Flavobacterium*, and a 4 % decline in *Pseudomonas*. Despite this, *Rhodobacter* and *Pseudomonas* remained dominant at this stage. The increased relative abundance of *Acetonaerobium* and *Macellibacteroides* indicated their role in supplying acetate and other volatile fatty acids (VFAs) to the system (Shi et al., 2023). The abundance of protein-hydrolyzing bacteria (*Proteiniphilum*) also significantly increased. These bacteria have been reported to convert proteins into VFAs (Lin et al., 2022), thereby enhancing carbon source utilization within the granules and contributing to the observed decrease in the PN/PS ratio.

In stage V, the abundance of salt-tolerant genera *Rhodobacter*, *Psychrobacter*, and *Arcobacter* significantly increased (Salas-Massó et al., 2016; Wang et al., 2020). Notably, *Psychrobacter* (23.8 %) overtook NaCl-sensitive *Pseudomonas* in abundance, becoming the second most dominant genus after *Rhodobacter* (30.8 %). This shift likely resulted from *Psychrobacter*'s halotolerance and its ability to grow on simple substrates such as short-chain fatty acids (Denner et al., 2001). Additionally, the abundance of protein-hydrolyzing genera such as *Proteiniphilum* and *Proteiniclasticum* further increased, potentially contributing to organic nitrogen turnover. However, TN became undetectable at this stage, indicating possible nitrogen depletion. This limitation likely favored nitrogen-fixing genera such as *Allorhizobium-Neorhizobium-Pararhizobium-Rhizobium*, which became increasingly dominant by stage VI (Huang et al., 2024). The decrease of protein-hydrolyzing bacteria may have been caused by the interaction between divalent metal ions and EPS, which inhibited protein hydrolysis. Meanwhile, the increased abundance of EPS-producing *Brevundimonas* suggests enhanced EPS secretion within the system. Overall, variations in environmental conditions at each stage, along with the adaptive capacity of microorganisms, collectively shaped the evolution of the community structure. Microorganisms grew and reproduced by adapting to their environment, while those unable to adapt were gradually eliminated.

### 3.4. COD removal and value-added products in the PSBR system

The COD removal performance of the reactor is shown in Fig. 5a. During the first two stages (days 0–57), the OLR was maintained at 0.75 kg COD/m<sup>3</sup>/d, in keeping with values for start-up of granular sludge reactors (Peyong et al., 2012). In stage I, the COD removal efficiency and biomass yield fluctuated between 77 and 85 % and 0.48–0.61 gbiomass/g COD<sub>removed</sub>, respectively, which was comparable to other suspended or biofilm-based PPB systems (Delamare-Deboutteville et al., 2019; Hao et al., 2024), with the effluent TN concentration remaining below 10 mg N/L. However, in stage II, the increased upflow velocity led to a shift in

**Table 2**

Diversity indices of the bacterial phylotypes in different operational stages.

Stage	OTU richness		OTU diversity		Coverage (%)
	Chao	ACE	Simpson	Shannon	
I	174.0	213.9	0.42	1.89	99.96
II	296.3	317.5	0.19	3.90	99.96
III	292.2	313.7	0.12	4.31	99.96
IV	307.6	342.7	0.10	4.35	99.95
V	298.4	314.0	0.16	3.75	99.97
VI	277.9	311.8	0.17	3.66	99.95

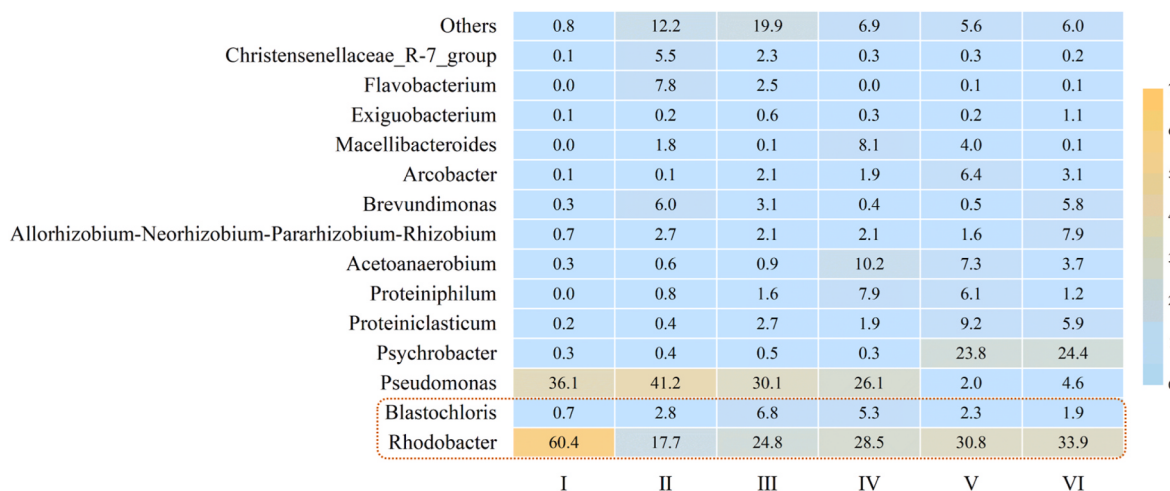


**Fig. 4.** Community composition at the gene level at the end of different stages of the operation. Stages I to VI correspond to: acclimation, upflow velocity increase (3.15 m/h), COD elevation, upflow velocity increase (4.5 m/h), sodium addition, and divalent ion addition, respectively.

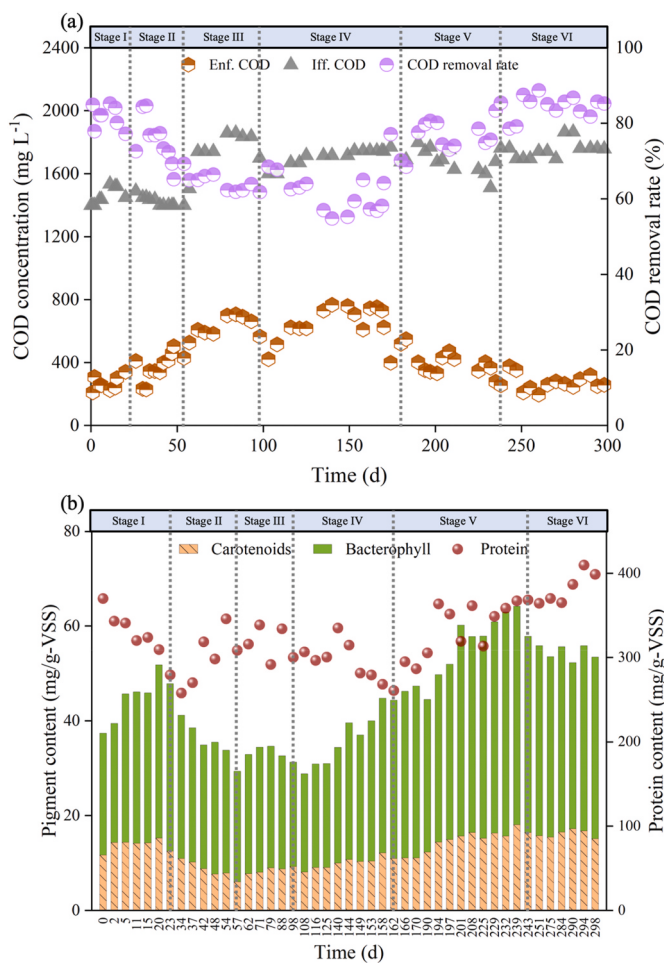


**Fig. 5.** The performance of the reactor in (a) COD removal and (b) production of carotenoids, bacteriochlorophylls, and protein. Stage I (acclimation), stage II (upflow velocity increased to 3.15 m/h), stage III (COD elevation), stage IV (upflow velocity increased to 4.5 m/h), stage V (sodium addition), and stage VI (divalent ion addition).

community structure and system instability. Meanwhile, the elevated biomass concentration and initial granule aggregation may have caused internal light limitation within the reactor, further inhibiting the

phototrophic activity of PPB. The COD removal efficiency declined to 69.34 %. After the OLR was increased to 0.9 kg COD/m<sup>3</sup>/d in stage III, the COD removal efficiency remained relatively stable, averaging 63.89 %. Following the increase in upflow velocity, a fluctuating trend was observed, with COD removal efficiency initially decreasing before recovering to 65.09 % by the end of stage IV. This pattern was likely due to the scouring of flocculent sludge and the restructuring of granular biomass. The excessive presence of flocculent sludge may have hindered COD uptake, whereas the restoration of granular structures improved system performance (Liu et al., 2018). In stage V, COD removal gradually increased and stabilized, indicating that sodium addition contributed to both system stability and enhanced substrate removal. Subsequently, in stage VI, COD removal further improved, reaching 84.41 % by day 298. The COD removal rate was approximately 0.75 kg COD/m<sup>3</sup>/d, which was comparable to previously reported values for PPB-based systems (Capson-Tojo et al., 2020). Meanwhile, the biomass yield reached 0.71 g<sub>biomass</sub>/g COD<sub>removed</sub>, and the effluent TN concentration became nearly undetectable, suggesting the onset of nitrogen limitation during the later stages. The notable improvement suggests that the porous granular structure induced by metal ions optimized substrate mass transfer and enhanced microbial utilization efficiency (Macêdo et al., 2019).

Since only PPB contained pigments in the system, pigment levels served as an indicator of PPB's photosynthetic capacity. Fig. 5b shows that pigment content remained abundant throughout most operational stages, except for stages III and IV, which were affected by flocculated sludge accumulation and subsequent recovery. This suggests that PPB maintained a favorable photosynthetic capacity throughout the process. After sodium addition (stage V), the pigment content (especially bacteriochlorophyll) increased significantly and reached a maximum of 64.18 mg/g VSS on day 239. The increase may be attributed to the antioxidant response induced by salt stress, wherein PPB enhances the synthesis of bacteriochlorophyll and carotenoids to counteract oxidative stress (Hao et al., 2024). Additionally, the presence of salt may stimulate hydrogenase activity and enhance photosystem I (PSI) cycling, further promoting bacteriochlorophyll synthesis (Wang et al., 2017).

Although SEM images showed that sodium-induced granules exhibited a compact morphology, the observed increase in pigment content suggests that pigment biosynthesis was not hindered by the granule structure. This may be attributed to the preferential localization of phototrophic microorganisms in the outer granule layers, where light is relatively more accessible (Liu et al., 2017). Indeed, Stegman et al. (2021) reported that PPB, such as *Rhodobacterales* and *Chromatiales*, were predominantly distributed within the outer ~100 µm of the

granules, with their abundance decreasing toward the core due to light attenuation. Although this spatial distribution was not directly assessed in our study, the sustained pigment accumulation under dense conditions indirectly supports this pattern. Similar enrichment of phototrophic or metabolically active populations in outer granule zones has also been observed in other systems (Abouhend et al., 2020; Billery et al., 2025; Trebuch, 2022). In contrast, the addition of calcium and magnesium did not directly stimulate pigment synthesis. Nevertheless, these ions likely contributed to the structural stability of the granules, thereby enhancing PPB retention and sustaining their photosynthetic metabolic activity.

Protein is also a value-added product with stable output in the PPB-based process. In this study, the highest protein content was observed at the end of the operation (399.1 mg/g VSS), exceeding that of the initial culture (370.3 mg/g VSS). Although this value was lower than previously reported protein levels in PPB granules (~590 mg/g VSS), the difference may be attributed to variations in strain composition and operating conditions (Capson-Tojo et al., 2020; Stegman et al., 2021). On the other hand, the apparent COD:N:P assimilation ratio in the system evolved from an initial 100:5.68:0.79 to 100:5.24:0.87 at the end of the operation. As nitrogen was completely depleted, this ratio did not represent the maximum assimilation potential of the system and was still below the optimal value of 100:6:1, which may have constrained further protein accumulation (Dalaei et al., 2020). Ammonium supplementation was not implemented during the operation in order to maintain consistent experimental conditions and avoid introducing additional variables. Nevertheless, the protein content of PPB granules in this study was comparable to that reported for algal-bacterial granular sludge (331–413 mg/g VSS) (Zhang et al., 2025). The results underscore the potential of PPB granules for protein recovery from wastewater, with further improvements possible through optimization of operational conditions and strain cultivation. However, it should be noted that the relatively high ash content (~50 %) observed in the granules may limit their direct use as microbial protein for feed applications. To improve their suitability for valorization, further processing, medium optimization (e.g., reducing inorganic buffer addition), or the use of real wastewater may be required to increase biomass purity.

### 3.5. Environmental relevance and implication

Granular sludge technology has been widely applied in wastewater treatment due to its high biomass concentration, excellent settling properties, and strong resistance to hydraulic and organic shock loads. Compared to other types of granules, PPB granules not only enable efficient pollutant removal but also offer resource recovery potential by producing high-value biomass products, thereby reducing treatment costs. However, PPB's reliance on light for growth, preference for a suspended state, and limited EPS secretion have hindered its granulation process. This study explored the synergistic effects of multiple strategies on PPB granule formation and examined their impact on pollutant removal and resource recovery.

The results demonstrated that increased upflow velocity facilitated the initial formation of PPB granules, while the addition of sodium and metal ions further promoted microbial aggregation and improved granule structure. Under optimized operating conditions, PSBR successfully cultivated PPB granules with superior settling properties, outperforming existing granulation techniques (Stegman et al., 2021). Compared to previous PPB granulation studies, flocculating microorganisms were substantially reduced, and the particle size distribution no longer exhibited a bimodal pattern. Meanwhile, the system maintained a high COD removal efficiency (84.41 %) and achieved substantial accumulation of protein (~40 %) and pigments (5.3 %), although slightly lower than those observed in the membrane reactor. The average particle size of PPB granules was relatively smaller than that of other granular technologies, primarily influenced by PPB's light absorption requirements. However, smaller granules may enhance substrate

transfer and COD uptake efficiency (Toja Ortega et al., 2022). Notably, PPB are also capable of synthesizing various high-value bioproducts, such as polyhydroxyalkanoates (PHA), coenzyme Q10 (CoQ10), and 5-aminolevulinic acid (5-ALA), which were not considered in the present study and warrant further investigation. In general, the high settling performance and stability of PPB granules suggest that they offer advantages over suspended and biofilm-based cultivation methods.

Although PPB granules exhibit promising stability and resource recovery potential, further optimization and validation are required for large-scale applications. On one hand, it is crucial to assess long-term granule stability and metabolic activity across different wastewater types and operational scales in practical engineering. To enhance PPB's competitiveness within microbial communities in complex wastewater environments, near-infrared light selection could be applied to maintain PPB dominance. On the other hand, the economic feasibility of PPB granulation remains a critical factor for large-scale implementation. Although PPB biomass has been recognized as a potential feed source for aquaculture (Delamare-Debouteville et al., 2019), the direct feeding of PPB granules has yet to be compared with pretreated PPB biomass (e.g., centrifugation, dehydration, and processing) in applications, and their relatively high ash content may require additional purification for feed use. Future research can be focused on optimizing granule formation strategies, increasing protein yield, and reducing operational costs to further evaluate the economic feasibility of PPB granules in wastewater treatment and resource recovery.

## 4. Conclusions

This study investigated the granulation process of PPB in a PSBR under multiple strategies and evaluated its performance in pollutant removal and resource recovery. The main conclusions are as follows.

1. PPB granules were successfully cultivated in the PSBR under optimized conditions, achieving a high settling velocity of 77.98 m/h, while flocculent sludge was almost eliminated.
2. Granulation was facilitated by stepwise increase in upflow velocity, with particle size distribution significantly improved from 3.15 to 4.5 m/h. Sodium and divalent metal ions enhanced granule aggregation and structural integrity by modulating EPS composition—sodium increased PS content, while calcium and magnesium increased PN content.
3. Microbial community analysis revealed dynamic succession during granulation. *Rhodobacter* and *Psychrobacter* dominated in the later stage, while EPS-associated genera such as *Brevundimonas* and *Flavobacterium* contributed to granule stability.
4. The PPB granules exhibited stable COD removal efficiency (84.41 %) and favorable accumulation of proteins (39.91 %) and pigments (5.34 %), demonstrating their feasibility for practical applications in wastewater treatment and resource recovery.

## CRediT authorship contribution statement

**Siwei Yu:** Writing – original draft, Methodology, Investigation, Formal analysis, Conceptualization. **Tianqi Hao:** Methodology, Investigation. **Xiaoshuai Peng:** Methodology, Formal analysis. **Yifeng Xu:** Supervision, Methodology, Funding acquisition. **Linchuan Fang:** Writing – review & editing, Supervision, Investigation. **Lai Peng:** Writing – review & editing, Supervision, Project administration, Investigation, Funding acquisition, Conceptualization.

## Declaration of competing interest

The authors declare that they have no known competing financial interests or personal relationships that could have appeared to influence the work reported in this paper.

## Acknowledgments

The authors thank the National Natural Science Foundation of China (No. 42477068), Shenzhen Science and Technology Program (No. JCYJ20230807121305010), the Foundation of Key Laboratory of Yangtze River Water Environment, Ministry of Education (Tongji University), China (No. YRWEF202302), Hubei Provincial Key Research and Development Program (No. 2022BCA067) and Knowledge Innovation Program of Wuhan-Shuguang Project (No. 2023020201020317) for supporting this study.

## Appendix A. Supplementary data

Supplementary data to this article can be found online at <https://doi.org/10.1016/j.jenvman.2025.126741>.

## Data availability

Data will be made available on request.

## References

- Abouhend, A.S., McNair, A., Kuo-Dahab, W.C., Watt, C., Butler, C.S., Milferstedt, K., Hamelin, J., Seo, J., Gikonyo, G.J., El-Moselhy, K.M., Park, C., 2018. The oxygenic photorgranule process for aeration-free wastewater treatment. *Environ. Sci. Technol.* 52, 3503–3511.
- Abouhend, A.S., Milferstedt, K., Hamelin, J., Ansari, A.A., Butler, C., Carbajal-González, B.I., Park, C., 2020. Growth progression of oxygenic photorgranules and its impact on bioactivity for aeration-free wastewater treatment. *Environ. Sci. Technol.* 54, 486–496.
- Alloul, A., Ganigüe, R., Spiller, M., Meerburg, F., Cagnetta, C., Rabaey, K., Vlaeminck, S.E., 2018. Capture-ferment-upgrade: a three-step approach for the valorization of sewage organics as commodities. *Environ. Sci. Technol.* 52, 6729–6742.
- Alloul, A., Wuyts, S., Lebeer, S., Vlaeminck, S.E., 2019. Volatile fatty acids impacting phototrophic growth kinetics of purple bacteria: paving the way for protein production on fermented wastewater. *Water Res.* 152, 138–147.
- American Public Health Association, A.P.H., 2017. Standard Methods for the Examination of Water and Wastewater, 9me 2. Creative Media Partners, LLC.
- Batstone, D.J., Keller, J., 2001. Variation of bulk properties of anaerobic granules with wastewater type. *Water Res.* 35, 1723–1729.
- Billary, C., Gaval, G., Hamelin, J., Milferstedt, K., 2025. Phototrophic aggregates for wastewater treatment: identifying key parameters for formation and characterization. *Rev. Environ. Sci. Biotechnol.* 24, 425–450.
- Capson-Tojo, G., Batstone, D.J., Grassino, M., Hülsken, T., 2022. Light attenuation in enriched purple phototrophic bacteria cultures: implications for modelling and reactor design. *Water Res.* 219, 118572.
- Capson-Tojo, G., Batstone, D.J., Grassino, M., Vlaeminck, S.E., Puyol, D., Verstraete, W., Kleerebezem, R., Oehmen, A., Ghimire, A., Pikaar, I., Lema, J.M., Hülsken, T., 2020. Purple phototrophic bacteria for resource recovery: challenges and opportunities. *Biotechnol. Adv.* 43, 107567.
- Capson-Tojo, G., Lin, S., Batstone, D.J., Hülsken, T., 2021. Purple phototrophic bacteria are outcompeted by aerobic heterotrophs in the presence of oxygen. *Water Res.* 194, 116941.
- Capson-Tojo, G., Zuo Meng Gan, A., Ledezma, P., Batstone, D.J., Hülsken, T., 2023. Resource recovery using enriched purple phototrophic bacteria in an outdoor flat plate photobioreactor: suspended vs. attached growth. *Bioresour. Technol.* 373, 128709.
- Cerruti, M., Stevens, B., Ebrahimi, S., Alloul, A., Vlaeminck, S.E., Weissbrodt, D.G., 2020. Enrichment and aggregation of purple non-sulfur bacteria in a mixed-culture sequencing-batch photobioreactor for biological nutrient removal from wastewater. *Front. Bioeng. Biotechnol.* 8, 557234.
- Chen, J., Wei, J., Ma, C., Yang, Z., Li, Z., Yang, X., Wang, M., Zhang, H., Hu, J., Zhang, C., 2020. Photosynthetic bacteria-based technology is a potential alternative to meet sustainable wastewater treatment requirement? *Environ. Int.* 137, 105417.
- Dalaei, P., Bahrani, G., Nakhla, G., Santoro, D., Batstone, D., Hülsken, T., 2020. Municipal wastewater treatment by purple phototrophic bacteria at low infrared irradiances using a photo-anaerobic membrane bioreactor. *Water Res.* 173, 115535.
- Delaware-Deboutteville, J., Batstone, D.J., Kawasaki, M., Stegman, S., Salini, M., Tabrett, S., Smullen, R., Barnes, A.C., Hülsken, T., 2019. Mixed culture purple phototrophic bacteria is an effective fishmeal replacement in aquaculture. *Water Res.* X 4, 100031.
- Denner, E.B.M., Mark, B., Mark, B., Busse, H.-J., Busse, H.-J., Turkiewicz, M., Lubitz, W., 2001. Psychrobacter proteolyticus sp. nov., a psychrotrophic, halotolerant bacterium isolated from the antarctic krill *Euphausia superba* Dana, excreting a cold-adapted metalloprotease. *Syst. Appl. Microbiol.* 24, 44–53.
- Ding, X.S., Zhao, B., An, Q., Tian, M., Guo, J.S., 2019. Role of extracellular polymeric substances in biofilm formation by *Pseudomonas stutzeri* strain XL-2. *Appl. Microbiol. Biotechnol.* 103, 9169–9180.
- Fang, F., Yang, M.-M., Wang, H., Yan, P., Chen, Y.-P., Guo, J.-S., 2018. Effect of high salinity in wastewater on surface properties of anammox granular sludge. *Chemosphere* 210, 366–375.
- Gagliano, M.C., Ismail, S.B., Stams, A.J.M., Plugge, C.M., Temmink, H., Van Lier, J.B., 2017. Biofilm formation and granule properties in anaerobic digestion at high salinity. *Water Res.* 121, 61–71.
- Hao, T., Xu, Y., Liang, C., Peng, X., Yu, S., Peng, L., 2024. Establishing an efficient membrane bioreactor for simultaneous pollutant removal and purple bacteria production under salinity stress. *Chemosphere* 353, 141535.
- Huang, H.-M., Xue, Z.-X., Jiang, Y.-F., Li, R., Guo, R.-B., Fan, X.-L., Fu, S.-F., 2024. New approach for raw biogas: production of single cell protein by sulfide-tolerant methane-oxidizing bacteria consortia. *Chem. Eng. J.* 495, 153678.
- Hülsken, T., Barry, E.M., Lu, Y., Puyol, D., Keller, J., Batstone, D.J., 2016. Domestic wastewater treatment with purple phototrophic bacteria using a novel continuous photo anaerobic membrane bioreactor. *Water Res.* 100, 486–495.
- Hülsken, T., Batstone, D.J., Keller, J., 2014. Phototrophic bacteria for nutrient recovery from domestic wastewater. *Water Res.* 50, 18–26.
- Imhoff, J.F., Dworkin, M., Falkow, S., Rosenberg, E., Schleifer, K.-H., Stackebrandt, E. (Eds.), 2006. The Prokaryotes. Springer-Verlag, pp. 41–64.
- Jiang, W., Wei, H., Xu, Z., Kang, J., Wang, S., Liu, D., Ren, Y., Ngo, H.H., Guo, W., Ye, Y., 2025. Lighting promotes sulfate removal and improves microbial community stability in upflow anaerobic sludge bed reactors under low ratio of chemical oxygen demand to sulfate. *Bioresour. Technol.* 428, 132473.
- Kolbeck, S., Abele, M., Hilgarth, M., Vogel, R.F., 2021. Comparative proteomics reveals the anaerobic lifestyle of meat-spoiling pseudomonas species. *Front. Microbiol.* 12, 2021.
- Kurzyna-Szklarek, M., Cybulski, J., Zdunek, A., 2022. Analysis of the chemical composition of natural carbohydrates – an overview of methods. *Food Chem.* 394, 133466.
- Li, H., Guo, J., Lian, J., Xi, Z., Song, Q., Song, Y., Han, Y., Lu, C., 2019. The modified mechanism for denitrifying granular sludge formation in a UASB reactor. *Desalination Water Treat.* 145, 26–35.
- Li, J., Hao, X., van Loosdrecht, M.C.M., Lin, Y., 2025. Understanding the ionic hydrogel-forming property of extracellular polymeric substances: differences in lipopolysaccharides between flocculent and granular sludge. *Water Res.* 268, 122707.
- Li, X.-M., Liu, Q.-Q., Yang, Q., Guo, L., Zeng, G.-M., Hu, J.-M., Zheng, W., 2009. Enhanced aerobic sludge granulation in sequencing batch reactor by Mg<sup>2+</sup> augmentation. *Bioresour. Technol.* 100, 64–67.
- Lin, L., Li, Z., Zhang, B., Zhang, Q., Qiu, D., Herzberg, M., Wu, Z., Xiao, E., 2022. Degradation and utilization of EPS from excessive activated sludge by interaction of electrogenesis and light stimulation. *J. Environ. Chem. Eng.* 10, 107557.
- Liu, L., Fan, H., Liu, Y., Liu, C., Huang, X., 2017. Development of algae-bacteria granular consortia in photo-sequencing batch reactor. *Bioresour. Technol.* 232, 64–71.
- Liu, L., Gao, D.-W., Zhang, M., Fu, Y., 2010. Comparison of Ca<sup>2+</sup> and Mg<sup>2+</sup> enhancing aerobic granulation in SBR. *J. Hazard. Mater.* 181, 382–387.
- Liu, P.-y., Chen, J.-r., Shao, L., Tan, J., Chen, D.-j., 2018. Responses of flocculent and granular sludge in anaerobic sequencing batch reactors (ASBRs) to azithromycin wastewater and its impact on microbial communities. *J. Chem. Technol. Biotechnol.* 93, 2341–2350.
- Liu, Y., Xu, H.-L., Yang, S.-F., Tay, J.-H., 2003. Mechanisms and models for anaerobic granulation in upflow anaerobic sludge blanket reactor. *Water Res.* 37, 661–673.
- Lowry, O., Rosebrough, N., Farr, A.L., Randall, R., 1951. Protein measurement with the folin phenol reagent. *J. Biol. Chem.* 193, 265–275.
- Lu, H., Dong, S., Zhang, G., Han, T., Zhang, Y., Li, B., 2019a. Enhancing the auto-flocculation of photosynthetic bacteria to realize biomass recovery in brewery wastewater treatment. *Environ. Technol.* 40, 2147–2156.
- Lu, H., Peng, M., Zhang, G., Li, B., Li, Y., 2019b. Brewery wastewater treatment and resource recovery through long term continuous-mode operation in pilot photosynthetic bacteria-membrane bioreactor. *Sci. Total Environ.* 646, 196–205.
- Macédo, W.V., Sakamoto, I.K., Azevedo, E.B., Damjanovic, M.H.R.Z., 2019. The effect of cations (Na<sup>+</sup>, Mg<sup>2+</sup>, and Ca<sup>2+</sup>) on the activity and structure of nitrifying and denitrifying bacterial communities. *Sci. Total Environ.* 679, 279–287.
- Meng, F., Yang, A.Q., Zhang, G.M., Wang, H.Y., 2017. Effects of dissolved oxygen concentration on photosynthetic bacteria wastewater treatment: pollutants removal, cell growth and pigments production. *Bioresour. Technol.* 241, 993–997.
- Peyong, Y.N., Zhou, Y., Abdullah, A.Z., Vadivelu, V., 2012. The effect of organic loading rates and nitrogenous compounds on the aerobic granules developed using low strength wastewater. *Biochem. Eng. J.* 67, 52–59.
- Ren, T.-T., Liu, L., Sheng, G.-P., Liu, X.-W., Yu, H.-Q., Zhang, M.-C., Zhu, J.-R., 2008. Calcium spatial distribution in aerobic granules and its effects on granule structure, strength and bioactivity. *Water Res.* 42, 3343–3352.
- Salas-Massó, N., Andree, K.B., Furones, M.D., Figueras, M.J., 2016. Enhanced recovery of *Arcobacter* spp. using NaCl in culture media and re-assessment of the traits of *Arcobacter marinus* and *Arcobacter halophilus* isolated from marine water and shellfish. *Sci. Total Environ.* 566–567, 1355–1361.
- Salmiati, Dahalan, F.A., Mohamed Najib, M.Z., Salim, M.R., Ujang, Z., 2015. Characteristics of developed granules containing phototrophic aerobic bacteria for minimizing carbon dioxide emission. *Int. Biodegrad.* 102, 15–23.
- Shaikh, S., Rashid, N., Onwusogh, U., McKay, G., Mackey, H.R., 2023. Effect of nutrients deficiency on biofilm formation and single cell protein production with a purple non-sulphur bacteria enriched culture. *Biofilm* 5, 100098.
- Shi, Y., Xue, H., Yao, Y., Jing, C., Liu, R., Niu, Q., Lu, H., 2023. Overcoming methanogenesis barrier to acid inhibition and enhancing PAHs removal by granular biochar during anaerobic digestion. *Chem. Eng. J.* 477, 147229.

- Stegman, S., Batstone, D.J., Rozendal, R., Jensen, P.D., Hulsen, T., 2021. Purple phototrophic bacteria granules under high and low upflow velocities. *Water Res.* 190, 116760.
- Toja Ortega, S., van den Berg, L., Pronk, M., de Kreuk, M.K., 2022. Hydrolysis capacity of different sized granules in a full-scale aerobic granular sludge (AGS) reactor. *Water Res.* X 16, 100151.
- Torres, K., Álvarez-Hornos, F.J., San-Valero, P., Gabaldón, C., Marzal, P., 2018. Granulation and microbial community dynamics in the chitosan-supplemented anaerobic treatment of wastewater polluted with organic solvents. *Water Res.* 130, 376–387.
- Trebuch, L.M., 2022. Photogranules for Wastewater Treatment : from Community Assembly to Targeted Microbial Functions. Wageningen University, Netherlands, p. 225.
- Trunk, K., Benkert, B., Quäck, N., Müinch, R., Scheer, M., Garbe, J., Jänsch, L., Trost, M., Wehland, J., Buer, J., Jahn, M., Schobert, M., Jahn, D., 2010. Anaerobic adaptation in *Pseudomonas aeruginosa*: definition of the Anr and Dnr regulons. *Environ. Microbiol.* 12, 1719–1733.
- Wan, C., Yang, X., Lee, D.-J., Liu, X., Sun, S., Chen, C., 2014. Partial nitrification of wastewaters with high NaCl concentrations by aerobic granules in continuous-flow reactor. *Bioresour. Technol.* 152, 1–6.
- Wang, H., Yang, A., Zhang, G., Ma, B., Meng, F., Peng, M., Wang, H., 2017. Enhancement of carotenoid and bacteriochlorophyll by high salinity stress in photosynthetic bacteria. *Int. Biodeterior. Biodegrad.* 121, 91–96.
- Wang, J., Liu, Q., Wu, B., Hu, H., Dong, D., Yin, J., Ren, H., 2020. Effect of salinity on mature wastewater treatment biofilm microbial community assembly and metabolite characteristics. *Sci. Total Environ.* 711, 134437.
- Wilén, B.-M., Liébana, R., Persson, F., Modin, O., Hermansson, M., 2018. The mechanisms of granulation of activated sludge in wastewater treatment, its optimization, and impact on effluent quality. *Appl. Microbiol. Biotechnol.* 102, 5005–5020.
- Yu, S., Peng, L., Xu, Y., Song, S., Xie, G.-J., Liu, Y., Ni, B.-J., 2021. Optimizing light sources for selective growth of purple bacteria and efficient formation of value-added products. *J. Clean. Prod.* 280, 124493.
- Zhang, B., Zhao, L., Ke, Z., Liu, Y., Wang, J., Huang, W., Yang, F., Huang, W., 2025. Nutrient reclamation from brackish and marine aquaculture wastewaters as fish feed additives using algal-bacterial granular sludge technology. *Chem. Eng. J.* 506, 160002.
- Zhang, L., Zhang, Y., Yuan, Y., Mou, A., Park, S., Liu, Y., 2022a. Impacts of granular activated carbon addition on anaerobic granulation in blackwater treatment. *Environ. Res.* 206, 112406.
- Zhang, M., Ji, B., Wang, S., Gu, J., Liu, Y., 2022b. Granule size informs the characteristics and performance of microalgal-bacterial granular sludge for wastewater treatment. *Bioresour. Technol.* 346, 126649.
- Zhou, Q., Zhang, P.Y., Zhang, G.M., 2014. Biomass and carotenoid production in photosynthetic bacteria wastewater treatment: effects of light intensity. *Bioresour. Technol.* 171, 330–335.